Available online at www.sciencedirect.com

jmr&t Journal of Materials Research and Technology

journal homepage: www.elsevier.com/locate/jmrt

Original Article

A machine learning enabled ultra-fine grain design strategy of Mg–Mn-based alloys

Xiaoxi Mi [a], *Xuerui Jing* [a], *Hailian Wang* [a], *Jianbin Xu* [c], *Jia She* [a,b], *Aitao Tang* [a,b,*], *Bjørn Holmedal* [c], *Fusheng Pan* [a,b]

[a] *College of Materials Science and Engineering, Chongqing University, Chongqing, China*
[b] *National Engineering Research Center for Magnesium Alloys, Chongqing University, Chongqing, China*
[c] *Department of Materials Science and Engineering, Norwegian University of Science and Technology (NTNU), Trondheim, Norway*

ARTICLE INFO

Article history:
Received 12 December 2022
Accepted 14 February 2023
Available online 22 February 2023

Keywords:
Mg–Mn-based alloy
Ultrafine grain
Machine learning
Classification
Prediction

ABSTRACT

Grain size is the critical characteristic of ultra-fine grain Magnesium (Mg), which is a concrete representation of the whole heat deformation procedure. In this paper, a design strategy was proposed to quantitatively investigate the composition and process conditions for the preparation of ultrafine grains. Herein, a dataset of Mg–Mn-based wrought alloys was constructed, and the average grain size was set as the design target. Based on this dataset, five machine learning (ML) algorithms, including the k-nearest neighbor (kNN), support vector machine (SVM), decision tree (DT), random forest (RF), and artificial neural network (ANN), were integrated to conduct in-depth analysis and make predictions. Among these models, the computational accuracy of both the DT classifier and ANN predictor is around 90%. The main factors affecting the formation of ultrafine grains were found by ML, and the interrelationships between the features were quantitatively analyzed as well. Then, four suggested routes with conditions were extracted from the tree models for preparing ultrafine grain Mg alloys. And four new Mg alloys were designed through these routes and taken as experimental validation. After testing, the actual grain sizes are close to the predictions, and the accuracy of the experimental verification exceeds 80%. Compared with conventional "trial and error" design methods, the grain design strategy proposed in this paper brings new thought and good prior guidance for developing high-performance commercial Mg alloys.

1. Introduction

Magnesium (Mg) and its alloys, with low density, high specific strength, high thermal conductivity, high damping, and good electromagnetic shielding properties, have become one of the most promising structural materials for applications [1,2]. However, the lower strength and poor ductility are still the main bottlenecks impeding their commercial applications

* Corresponding author.
E-mail address: tat@cqu.edu.cn (A. Tang).
https://doi.org/10.1016/j.jmrt.2023.02.091

[3,4]. Grain refinement is the most effective way to enhance strength and plasticity simultaneously. Grain refining will significantly increase the strength and ductility of wrought Mg, especially when the grain size approaches several microns (ultrafine scale) [5–7]. Therefore, ultra-fine grain fabrication is an important research direction for developing new high-performance commercial Mg alloys. Some severe plastic deformation technologies have been reported, such as high-pressure torsion (HPT) [8,9], equal channel angular pressing (ECAP) [10,11], accumulative roll bonding (ARB) [12,13], multidirectional forging (MF) [14], which are possible to prepare ultra-fine grain structures. Nevertheless, they are either techniques complex, costly, or not suitable for large-scale industrial production. Hence, the research on obtaining ultra-finegrain Mg alloys by a simple deformation procedure with good properties is essential to expand their applications.

Recently, Mg–Mn-based ultra-fine grain alloys have been drawing significant attention in the development of new commercial Mg due to their low cost, straightforward production process, and superior performance [15–17]. Several commercially available Mn-containing Mg alloys, such as AZ31, AM50, AM60, ZM61, ZM91, and AMZ series alloys, have already been widely used in structural materials, the automotive industry, construction, rail transportation, and biological applications. Mg–Al–Zn and Mg–Al–Mn series alloys tend to have better plasticity, with fracture elongation reaching 15–25%, while Mg–Zn–Mn and Mg–Al–Mn–Zn series alloys boast higher strength, such as a ZM61 alloy processed through conventional extrusion with a reported yield and ultimate tensile strength of 320 MPa and 350 MPa, respectively [1–4,17–20]. The formation of ultrafine grain structure in Mg–Mn-based alloys is achieved through the promotion of dynamic recrystallization and the inhibition of grain growth. The primary alloying elements, including Mn, Al, Zn, Sn, and Ca, provide two key benefits in the preparation of ultrafine grain structures: first, the precipitation of solid solution elements, particularly α-Mn, generates numerous nuclei for recrystallization during thermal deformation, boosting the driving force of recrystallization. The precipitation of delicate second phases also restrict grain boundary migration and further refines the recrystallization grains. Second, these alloying elements enhance the deformability of the alloy at low and medium temperatures (typically between 200 °C and 400 °C), allowing it to be processed through conventional extrusion at lower temperatures and inhibiting the growth of recrystallized grains. Furthermore, the Mg–Mn-based alloy is more economically feasible compared to Mg-Rare earth alloys with similar mechanical properties, making it a more attractive option for large-scale industrial production [21–25].

However, there are two thorny issues in developing new Mg–Mn-based wrought alloys: Firstly, the design of Mg–Mn-based alloys still mainly relies on the trial-and-error method, which is unpredictable, low-yielding, and high-cost. Especially when there are many variables of alloying elements and extrusion process parameters, it is difficult to describe the complex relationships between these variables accurately and systematically. Secondly, by comparing some research works, Mg alloys with ultrafine grain structures tend to perform better even in the same alloy system. However, not all Mn-containing wrought Mg alloys have ultrafine grain structures and various factors could influence grain size. Besides the alloying elements, the deformation temperature and rate are also influential [26–28]. Therefore, more systematic and quantitative studies on how to prepare ultrafine grains are still needed.

Over the past decade, machine learning (ML) has gained significant attention and momentum in the field of materials science [29–32]. As a data-driven technology, ML can help users extract information from data, build relationships, and make judgments [33–36]. ML has also been applied to microstructure analysis, characterization, and design. For example, Orme and Tong used a decision tree framework to mine information from AZ31 EBSD data and explore the correlation between physical properties and twinning [37,38]. Doo Jung used artificial neural network models to find a quantitative relationship between steel structures and mechanical properties and successfully designed the high strength steels [39]. Fang used a convolutional neural network data-driven framework to automatically extract the dominant predictive features from simulated temperature history. Perfect predictions of material properties, especially ultimate tensile strength, are obtained using simulated thermal history data [40]. ML is a practical method for alloy design that enables quantitative studies of alloy microstructures as long as suitable feature descriptors can be extracted. It is possible to design alloys effectively without comprehensive experiments. However, the microstructure of alloys often contains multiple structural features, which makes it challenging to accurately count a large amount of data and establish features with consistent criteria. As a result, current structural design methods for alloys are typically limited to designing for a single structural feature, such as grain size, texture intensity, or second phase morphology, etc.

In this paper, we propose a design strategy that integrates five machine learning algorithms to better understand the "composition-process-microstructure-property" relationship of ultrafine grain wrought Mg alloys. The workflow of this strategy is shown in Fig. 1. The average grain size was set as the critical target. Four classifiers were built using kNN, DT, SVM, and RF algorithms to predict grain types. We also obtained the composition and process parameter routes for preparing ultrafine grains using decision tree diagrams. In addition, a backward propagation artificial neural network (BP-ANN) model was built to predict the grain size (GS) with an accuracy of approximately 90%. Finally, we designed four target-possible alloys from four routes and made some experimental validations to evaluate the model performance, and the experimental results are in good agreement with the calculated results.

2. Dataset and features

2.1. *Dataset*

There are 163 sets collected from papers and previous experiments and organized into an Mg–Mn-based wrought alloy dataset [2–4,15–27,41–49]. All the alloys were extruded from

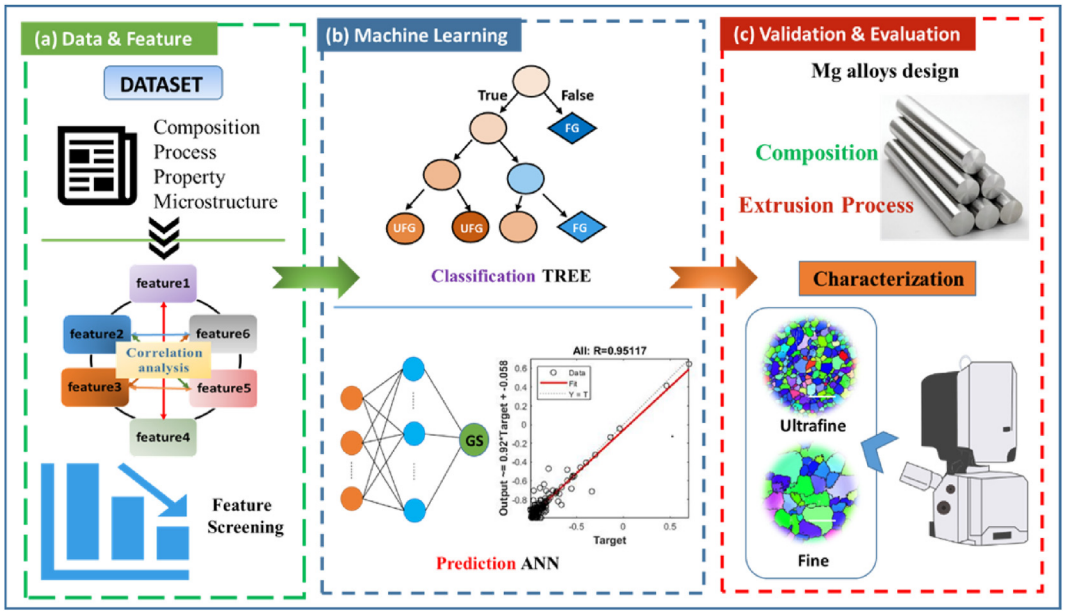

Fig. 1 – Schematic of the ultrafine grain design strategy for Mg–Mn-based wrought alloys.

ingots into rods after a short time of preheating. Five elements, Mn, Al, Zn, Sn, and Ca were denoted as the alloying composition features: They are the most common non-rare earth elements reported in the literature of ultrafine grain Mg, which are cheaper than rare earth elements and can make ingots easier extrude by conventional procedure. The dataset includes binary to quinary systems, each with a certain amount of Mn in the alloy. Extrusion temperature (ET, °C) and extrusion speed (ES, m/min) are chosen as features of process parameters [26–28]. Tensile yield strength (TYS), ultimate tensile strength (UTS) and fracture elongation (FE) are key indicators of the mechanical properties.

From a theoretical perspective, the microstructure of an alloy encompasses various elements, including grain homogeneity, grain size, texture intensity, the degree of recrystallization, as well as the distribution, size, and quantity of secondary phases. These microstructural characteristics ultimately dictate the properties of the alloys. However, in most Mg–Mn-based alloys, the microstructure after hot extrusion consists of numerous recrystallized grains. This recrystallization results in a uniform fine grain structure and weak texture due to the absence of elongated grains along the extrusion direction. Furthermore, as previously mentioned in introduction, the presence of fine and diffusely distributed second phases can promote dynamic recrystallization and inhibit the growth of recrystallized grains by pinning their boundaries. The stronger the effect of the second phases, the finer the recrystallized grains will be. In conclusion, the average grain size of recrystallization is a key determinant of the overall microstructure in the alloy systems covered in this paper. It is a result of the combined effect of various factors and provides a comprehensive representation of the microstructural characteristics. Thus, in this study we focused on average grain size (AGS) as the sole feature of microstructure. Table 1 provides definitions and the respective ranges for each of these features.

Table 1 – Definitions and ranges of features.

	Features	Range
Composition	Mn (wt.%)	0–3.0
	Al (wt.%)	0–8.9
	Zn (wt.%)	0–8.0
	Sn (wt.%)	0–5.0
	Ca (wt.%)	0–0.9
Extrusion parameter	Extrusion temperature (°C)	175–500
	Extrusion speed (m/min)	0.2–60.0
Microstructure	Average grain size (μm)	0.25–85.00
Mechanical property	Tensile yield strength (MPa)	95.0–403.0
	Ultimate tensile strength (MPa)	164.0–437.0
	Fracture elongation (%)	2.9–55.0

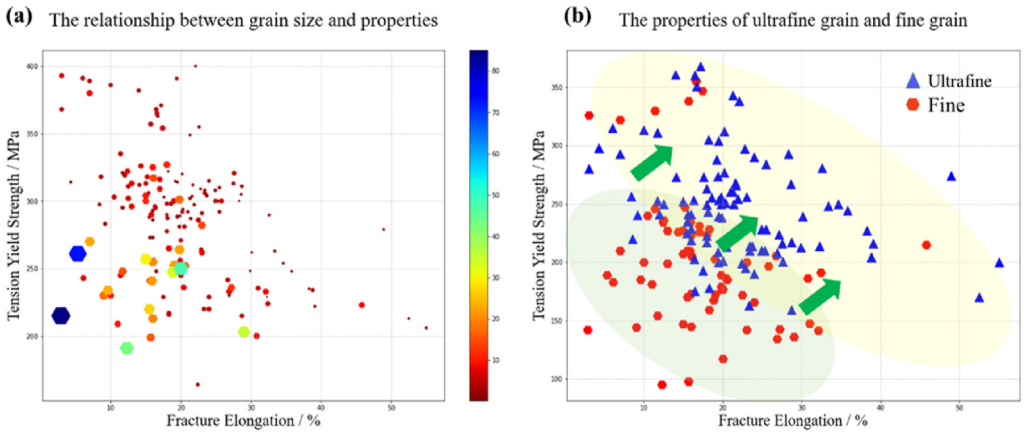

Fig. 2 – Relationships between mechanical properties and grains of Mg alloys.

2.2. *Relationships between features*

As mentioned, the most important mechanism of strengthening and toughening for Mg–Mn-based alloys is grain refining. All data from dataset were plotted in Fig. 2 with tension yield strength (MPa) as the vertical coordinate and fracture elongation (%) as the horizontal coordinate. Fig. 2(a) depicts the relationship between the grain size of these alloys and their mechanical properties. The size and color of the dots represent their average grain size, It can be observed that the performance improves as their AGS decreases, which aligns with the fine-grain strengthening theory. Furthermore, smaller grains are distributed near the diagonal line from the top left to the bottom right, while larger grains are concentrated at the bottom left of this line, indicating a clustering tendency.

Based on the characteristic of poly-crystalline metallic materials, an alloy with an AGS of 100 nm–1 μm is generally defined as the ultrafine grain alloy [50,51]. In ultrafine grain steels [52,53], it is generally considered that obtaining ultrafine grains is a refinement of the average grain size from the conventional tens of microns to around 1 μm. In steel materials, ultrafine grain structure can significantly improve, or even double its properties. For Mg, several studies have proved that when the AGS in Mg is below 5 μm, grain boundary slip starts to participate heavily in deformation. Meanwhile, the twinning behavior is suppressed. When the grain size is further reduced, the non-basal slip can be turned on to coordinate the deformation [54–56]. Due to the change of deformation mechanism, a more accepted term is that alloys with a uniform structure and an AGS below 5 μm are also referred to as ultrafine grain Mg. Therefore, combined with the general definition, ultrafine grain Mg alloy can be defined as the Mg with an AGS of 100 nm-5 μm [16,20,25,57,58]. In Fig. 2(b), we plotted all the data, where blue dots represent ultrafine grains with AGSs below 5 μm and red ones represent fine grains (AGS $\geq$ 5 μm). In this figure, the mechanical properties of the alloys are significantly improved from the fine grain to the ultra-fine grain region. This indicates that when designing new Mg, there is a higher probability of obtaining an alloy with better performance, especially the comprehensive mechanical properties, by intentionally controlling the grains to be ultrafine. In other words, grain ultra-fining is the practical means for further improving the performance of Mn-containing Mg. Based on the above, we focused on finding regulations to prepare ultrafine grains and how to predict them without needing any experiments.

Fig. 3 shows pair plots between elemental content, process parameters and grain size for all data. And each subplot illustrates the correlation between any two features. After fitting, we found that the effect of each feature (alloying elements and extrusion conditions) on grain size is nonlinear, which indicates that the formation of ultrafine structure is not influenced by single or double factors, nor a simple linear monotonous, but the result of the interaction of multiple factors. Therefore, we used machine learning algorithms that can handle high-dimensional and nonlinear problems to find relationships between features and further investigate the rules for preparing ultrafine microstructures.

3. Modeling and results

3.1. *Binary classifiers of grains*

We abstracted the ultrafine grain design as a binary supervised classification problem, where the input features are Mn, Al, Zn, Sn, Ca, ET and ES, and the output labels are *Ultrafine* and *Fine*. We wanted to verify the classification ability of the dataset by ML-classified models and determine if it is possible to separate ultrafine grains from fine grains in a multidimensional space based on their compositions and processing processes. If the data are separable, then we can find the spatial hyperplane that divides them, and this can help us identify the compositions and process routes for preparing ultrafine grain Mg alloys, as well as provide more insights into the formation of ultrafine structures. In that case, it is possible to find the composition and process routes for preparing ultrafine grain Mg alloys and more details about the formation of ultrafine grain structures.

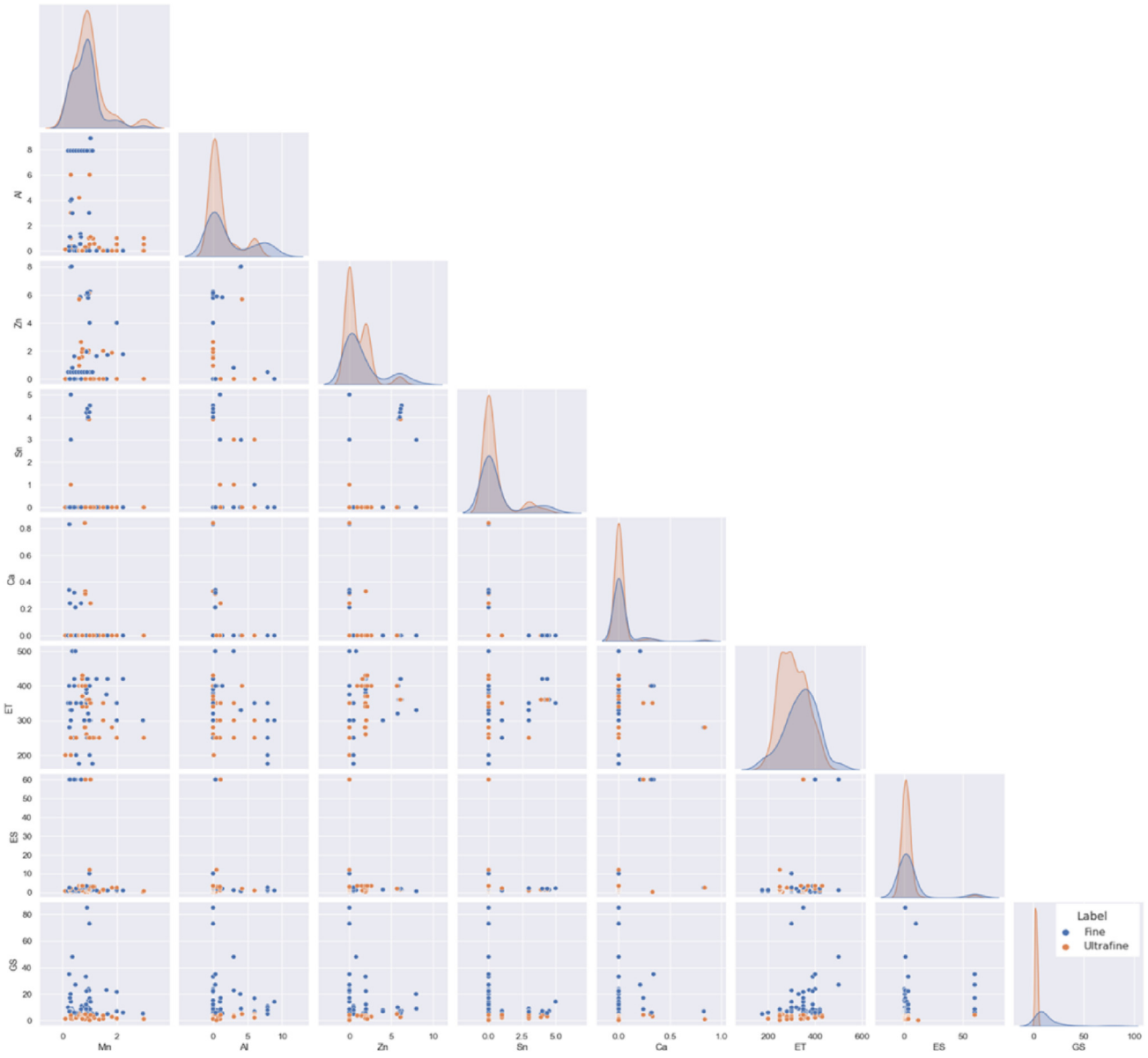

Fig. 3 – Pair plots between features and grain size.

Four ML algorithms, kNN, DT, SVM, and RF, were used to build classification models. The test set size for all models was 0.2, and the cross-validation approach was used for training and testing. The best parameters for the four ML models were optimized using the 'GridSearchCV' command and an enumeration circulation method. The parameters were set as the 'k = 5' in kNN, 'max_depth = 8' in DT, 'n_estimators = 100, max_depth = 7' in RF, and 'kernel = 'rbf', C = 5, gamma = 0.1' in SVM models, respectively. All the machine learning algorithms in this work come from the scikit-learn library based on Python [59].

The learning curves of the four classifiers shown in Fig. 4. In these figures, the red curve represents the training accuracy, the green one represents the cross-validation test accuracy, and the horizontal coordinates represent the proportion of the data used for training and testing in the dataset. As the data volume increase, the training accuracy starts from overfitting and gradually decreases to stable, while the testing accuracy gradually increases. All models eventually converge and are not overfitted. The test accuracy of all models is above 0.6, indicating that the composition and process can indeed determine the formation of ultrafine grains and fine grains, and it is probable to make ultrafine grains by controlling these parameters. Among them, the DT and RF models have higher accuracy, with training accuracy above 0.9 and testing accuracy of nearly 0.8. This suggests that the classification tree is more effective than the kNN and the SVM algorithms. In addition, compared to most algorithms, the decision tree model is not a complete black box; the decision tree nodes can be computed, and a tree diagram can show the whole classified workflow. Because of this advantage, the decision tree model is often used to find classification

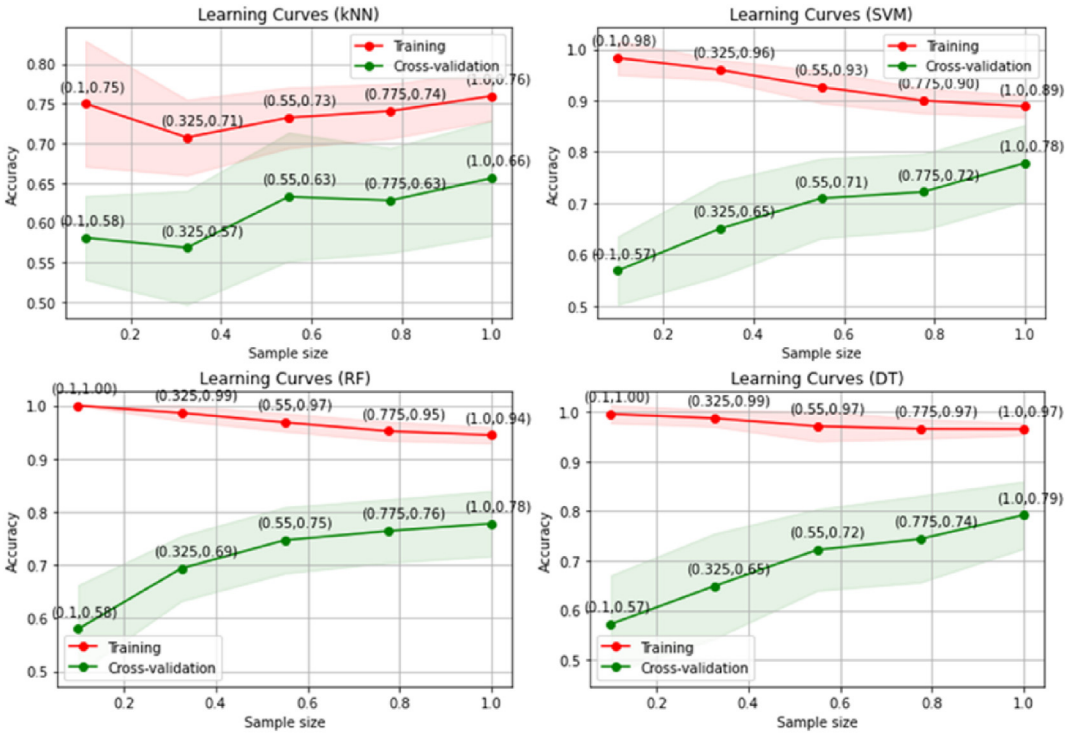

Fig. 4 – Learning curves of four classification models.

criteria and routes [37,38,60]. Therefore, we visualized the decision tree model in the next part to further explore paths to prepare ultrafine grains.

In order to investigate the influence of features on the target and improve the performance of the classification tree, we conducted feature screening and main feature analysis. We constructed and optimized a classification tree with a training accuracy of 0.94 and a test accuracy of 0.88. The mean decrease in impurity method was used to evaluate the importance of features influencing grain size. The results are shown in Fig. 5, in which the blue bars are the feature importance of the tree, along with their inter-tree variability represented by the error bars. When we classify all samples in fine and ultrafine grains, the feature importance of Al, ET, Mn, Zn, Sn, Ca, and ES is 0.32, 0.28, 0.21, 0.16, 0.03, 0, and 0, respectively. As can be seen from the feature weights, the most significant factors affecting the grain size are Al and ET, followed by Mn and Zn. In contrast, the effects of Sn, Ca, and

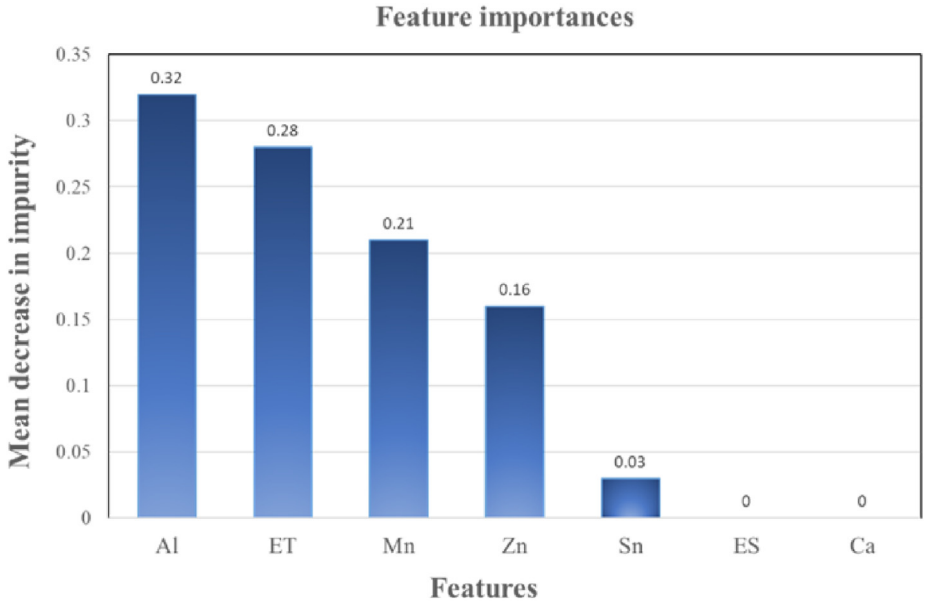

Fig. 5 – Feature importance of decision tree.

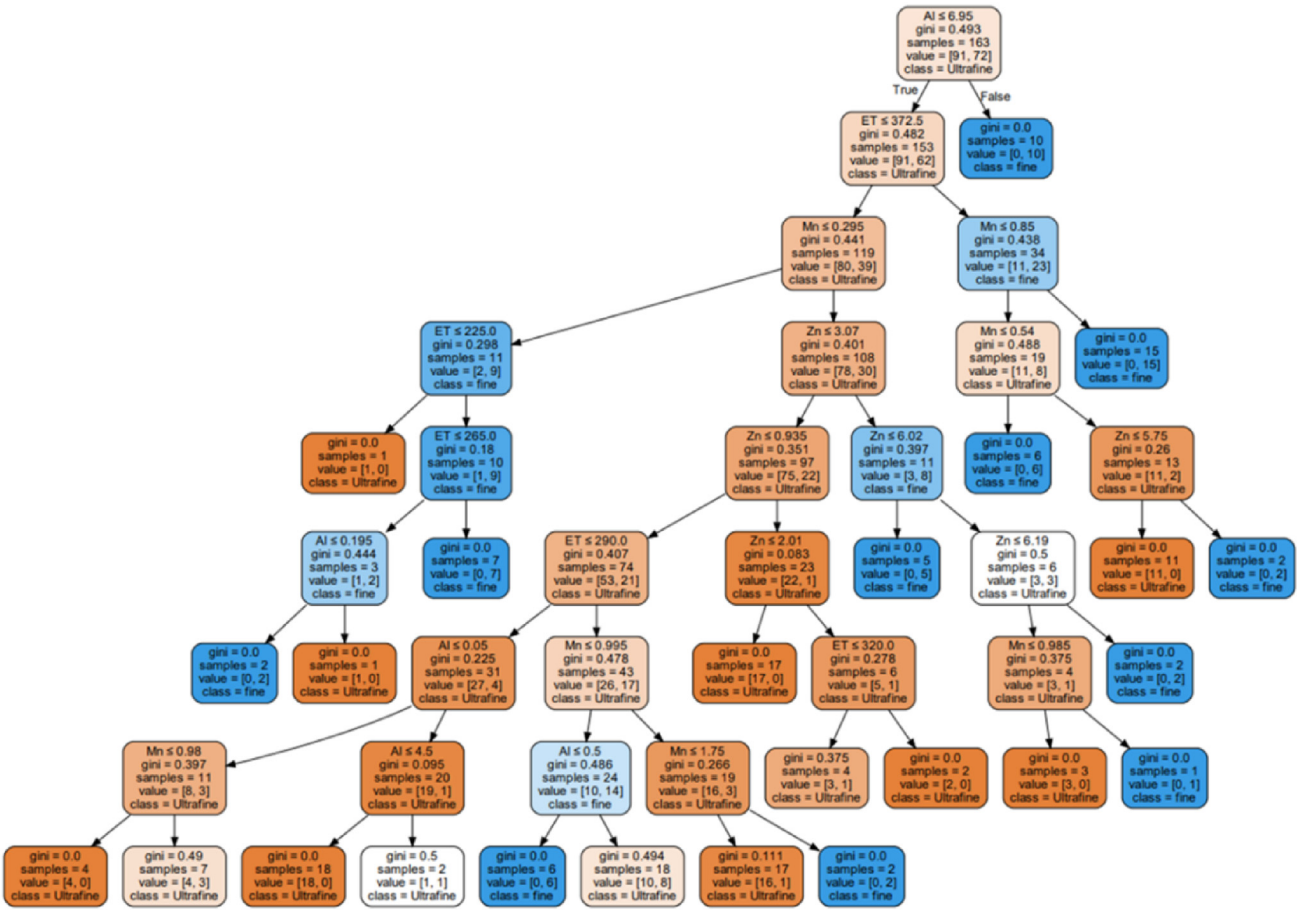

Fig. 6 – The classification tree for separating ultrafine and fine grains.

ES on the grain type are negligible. Therefore, in the subsequent visualization of the classification tree, only Al, ET, Mn and Zn features were kept, which helped to improve the model performance and reduced the interference branches.

After conducting feature screening and modeling optimization, the final tree model was built with input features of Al, Mn, Zn, ET, *Fine* and *Ultrafine* were set as labels. The depth of the decision tree is 7, the test size is 0.2, and the algorithm kernel is CART, whose training accuracy and testing accuracy are further improved to 0.95 and 0.91, respectively. This model can predict the grain type for any combination of the input features. Visualizing the decision tree allows us to find classified features and criteria values. Then, we used all the data as samples to generate the final classification tree, as shown in Fig. 6. The Gini index is a measure of classification accuracy that ranges from 0 to 1, with a lower value indicating a more accurate classification. In the decision tree, the node colors of yellow and blue represent ultrafine and fine grains, respectively. The node colors of yellow and blue families are used to represent ultrafine and fine grains respectively, and the darker the color indicates the smaller the gini coefficient, i.e., the more obvious the classification effect. The root node in the tree contains 163 samples, 91 of which are ultrafine grains and 72 are fine grains. There were 10 samples of alloy composition with Al content higher than 6.95 wt%, and all were fine grains. This indicates that the primary condition for obtaining ultrafine microstructure is to keep the Al content below 6.95 wt%. In the internal node of extrusion temperature, the critical value is 372.5. However, unlike the root node, it is still possible to prepare ultrafine grains by controlling other variables at the extrusion temperatures above or below 372.5 °C, as seen in the third-stage branches of the tree. In this way, there are 24 leaf nodes stemming from the root node, with each of them represents a route for producing ultrafine or fine grains. These leaf nodes have different sample sizes and labels. While a small-size leaf node may improve the classification performance, it is prone to overfitting and should be discarded. Finally, after screening and branch cutting, only four leaf nodes with ultrafine labels and a sample size greater than 10 were retained, indicating four routes for ultrafine grain preparation.

As shown in Fig. 6, each branch represents one route to design ultrafine or fine grain alloys. After pruning, we obtained four routes for preparing ultrafine grain Mg, as shown in Fig. 7. The condition values mainly come from the classification tree. However, the left and right boundaries are unclear for some conditions, and the extremums in the data were set as the critical values. The figure shows that in the Mg–Mn–Al–Zn system, the content of Al below 6.95% is the basic guideline for the preparation of ultrafine grain. There are

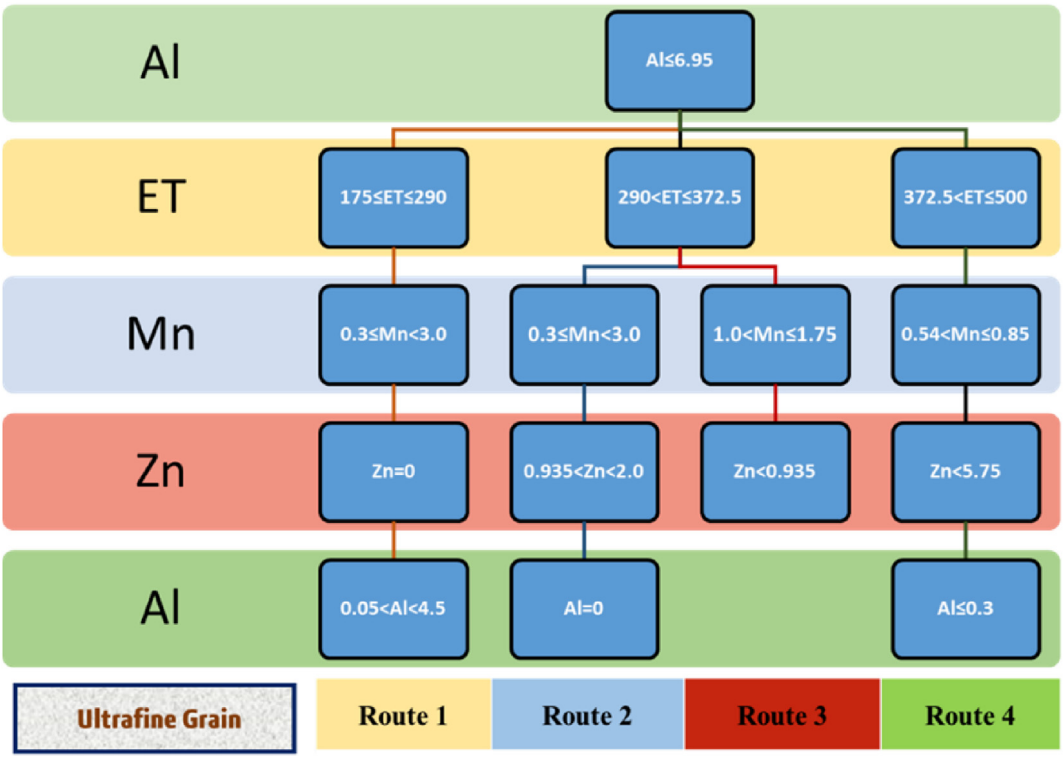

Fig. 7 – Routes for designing ultrafine grain from decision trees.

three extrusion temperature intervals can be chosen: the lower extrusion temperature ranges from 175 °C to 290 °C, the medium extrusion temperature ranges from 290 °C to 372.5 °C, and the higher extrusion temperature ranges above 372.5 °C. For route 1, the content of Zn needs to be controlled by no more than 0.935 wt% from the classification tree. Additionally, it was found that for all samples meeting other conditions of route 1, the content of Zn is 0, based on data from the dataset. This suggests that the alloys prepared by route 1 are the Mg–Mn–Al system. For route 2, similar to route 1, the content of Al is 0, which indicates that the alloys prepared using route 2 are the Mg–Mn–Zn system. For routes 3 and 4, there is no strict limitation to the number of alloy elements, and they can be ternary or quaternary, either. From these routes, there are some rules for the preparation of ultrafine grains of Mg alloys.

(1). The extrusion temperature must be increased with the increase of Zn content within the alloy system. When Zn = 0, as in the case of the Mg–Mn–Al-system alloy provided by route 1, extrusion at a lower temperature is necessary to obtain ultrafine grains. In subsequent experiments, the authors attempted to extrude the alloys of routes 2 to 4 at 280 °C, but were unable to do so. Therefore, it is crucial to match the extrusion temperature with the Zn content in the alloy when setting the extrusion temperature.

(2). Although the ultimate solid solution of elemental Al in the magnesium matrix is 12.7% (437 °C), the Al content is limited in all routes, particularly in route 2 and route 4. According to some previous studies [20,22,41,49], Al is more present in Mg–Al and Mn–Al fine second phases rather than in solid solution, which suggests that the main reason for the formation of the ultrafine structure is the action of the tiny second phases in the system.

(3). The relationship between Mn content and extrusion temperature shows an opposite trend to that of Zn. The lower the Mn content, the wider the extrusion temperature interval can be chosen. However, to obtain an ultra-fine structure, the Mn content should be at most 3 wt %.

Next, the data that satisfy each of the four process routes were plotted by their properties. As shown in Fig. 8, the alloy obtained by route 1 has a relatively higher fracture elongation, indicating that alloys with higher plasticity potential can be obtained through similar process routes. Similarly, the alloys obtained through routes 2 and 4 have higher strength potential, while the alloys obtained through route 3 may have more balanced mechanical properties. This information provides us with an effective guide for designing new Mg alloys. For example, when we want to obtain a wrought Mg alloy with ultimate tensile strength and fracture elongation over 200 MPa and 40%, our desired properties are within the range of route 1, and by choosing a lower extrusion temperature, 175–290 °C, and controlling the composition to be $0.05 < Al < 4.5$, $0.3 \leq Mn < 3.0$ and $Zn = 0$, there is a great probability of an ultrafine grain Mg alloy that meets the target properties. Finally, an Mg alloy microstructure design strategy with a fine grain strengthening theoretical basis and classification machine learning algorithms has been implemented.

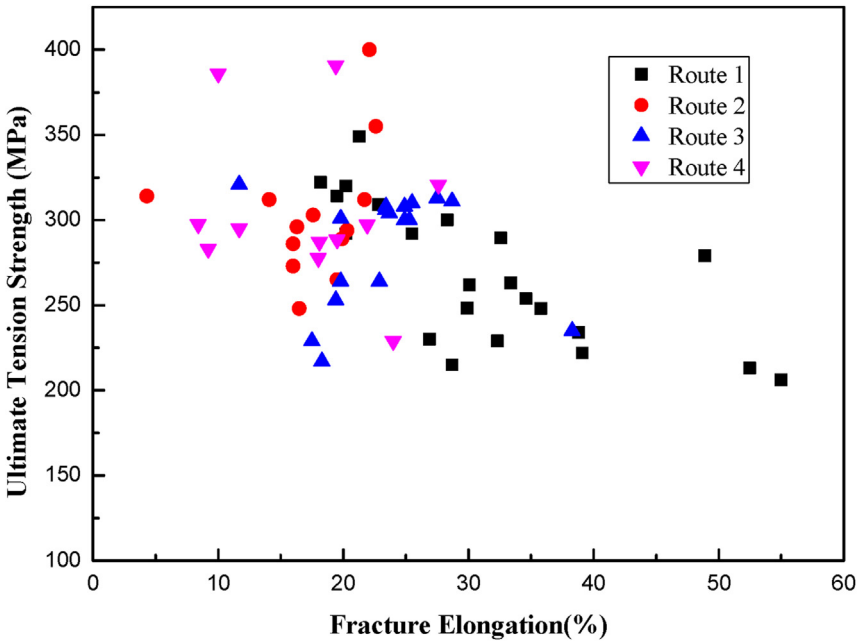

Fig. 8 – The performance of alloys through four routes.

3.2. *The grain size predictor*

In the previous sections, a classifier was used to predict the grain type and identify routes for preparing ultrafine grains, providing a priori guidance for developing new high-performance Mg alloys. In this part, a predictor was built to predict more precisely about grain size. From Figs. 2 and 3, it can be seen that the relationships between all parameters are nonlinear and multivariate. Artificial neural network (ANN) is the most popular and commonly used algorithm in modern ML, and are able to simulate complex nonlinear problems by combining linear transformation and nonlinear activation functions like human brains [61,62].

Here, we present a fully connected back propagation ANN (BP-ANN) that reflect the relationship between alloy compositions, extrusion process parameters and grain size. The BP-ANN, shown in Fig. 9, has seven neurons in the input layer, representing Mn, Al, Zn, Sn, Ca, ET, and ES. The single output layer has one neuron, which represents the grain size. The number of neurons in the hidden layer is determined using a loop-iteration method, where we substitute values from 5 to 20 in the model to find the convergent one with the lowest error. The approximate value range can be computed using empirical formulas. Furthermore, the optimal number of neurons in the hidden layer of the grain size prediction models is 13. The best optimization parameters were

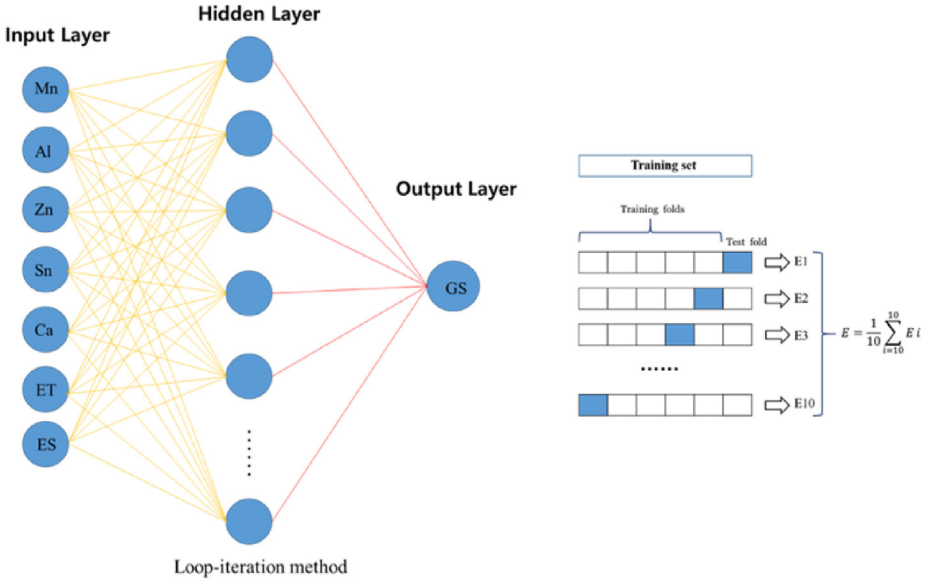

Fig. 9 – The structure of the BP-ANN model.

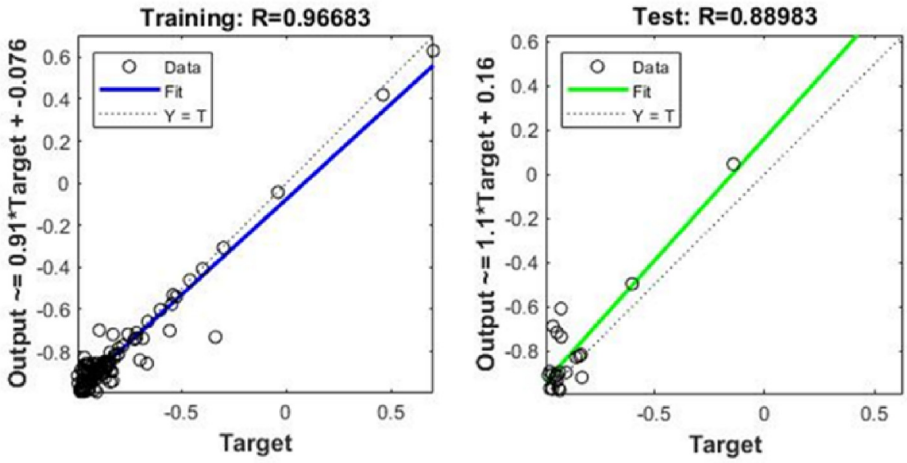

Fig. 10 – The regression results of the predictive BP-ANN model.

determined following multiple attempts. Selected "tansig" as an activation function, and the model was trained using normalization and the Bayesian regularization optimization, which can reduce the difficulty of optimizing the network and improve generalization. We set the proportion of the test data to 10% and used 10-fold cross-validation to optimize the division of the dataset. The maximum training epochs and the training accuracy were set to 1000 and 0.001, respectively.

After considerable training and testing, the fitting results of the ANN model are presented in Fig. 10. The regression values (R) of the training and test sets are 0.97, and 0.89, respectively, and the model is not over-fitted. The scattered points in these figures are concentrated and evenly distributed to the straight-line "Y = T", showing that the ANN model has a high degree of fitting and excellent generalization capability. The error histograms of models are shown in Fig. 11, which demonstrates that the error distributions are close to the normal distribution and the model errors mainly concentrate in the range of ±1.5 μm. This predictor can be used to predict the grain size of alloys with any inputs of compositions and extrusion processes.

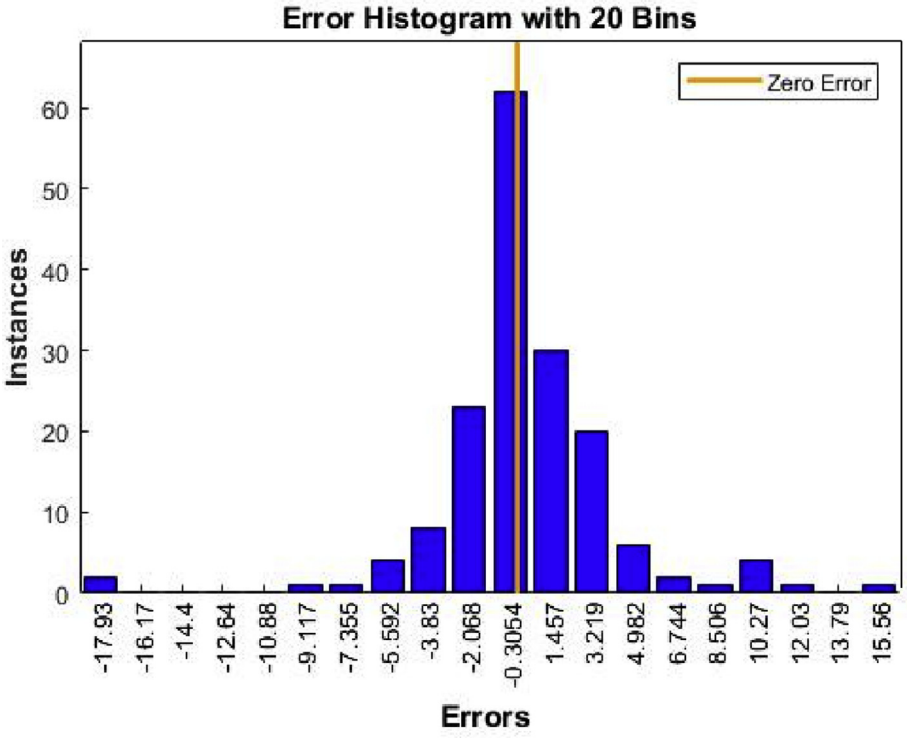

Fig. 11 – The error histograms of the BP-ANN model.

Table 2 – The compositions and processes of designing alloys.

No.	Composition and extrusion process			
Alloy	Mn/wt.%	Al/wt.%	Zn/wt.%	ET/°C
#1	1.0	0.3	0	280
#2	1.2	0	2.0	355
#3	1.1	3.0	0.9	310
#4	0.8	0.2	4.0	380

4. Experimental validation and model evaluation

As described above, the ultrafine grain Mg alloys can be designed using the four routes shown in Fig. 7. The properties of alloys prepared by these routes are also different. Therefore, we combined the classification tree and the ANN model to design several Mg alloys through each route, and then fabricated the alloys and performed some experimental tests. We randomly selected one component and one process parameter from each route as a sampling validation. The compositions and extrusion processes of four Mg alloys are shown in Table 2, denoted as #1, #2, #3 and #4, respectively.

Four alloys were produced according to the alloy design scheme given in Table 2. The ingots were prepared from high-purity Mg (>99.98 wt %), pure Al (>99.8 wt %), pure Zn (>99.9 wt %), and Mg–3Mn (wt. %) master alloys. The alloying components were completely melted in a steel crucible under the mixture gas of CO_2 (99.99 vol %) and SF_6 (1 vol %) at approximately 720 °C, and then water-cooled to form ingots. After cutting the surface defects and stains, ingots #1, #2, #3, and #4 were machined to obtain 80 mm diameter heights for extrusion without any pre-heat treatment. The ingots were hot extruded at 280 °C, 355 °C, 310 °C, and 380 °C using an XJ-500 horizontal extruder. As previously concluded, the effect of extrusion speed on grain size is very small for the alloy systems covered in this paper, so the extrusion speed of all designed alloys was set to 2.0 m/min (the median of the data). This resulted in the production of four rods with 16 mm diameters. After fabricating the alloys, some characterization experiments were performed. The grain structure was characterized using electron backscatter diffraction (EBSD) on the a JEOL JSM-7800F instrument with a scan step size of 0.4 μm. The microstructure of all as-extruded samples was observed parallel to the extrusion direction (ED), and analyzed using HKL Channel 5 software.

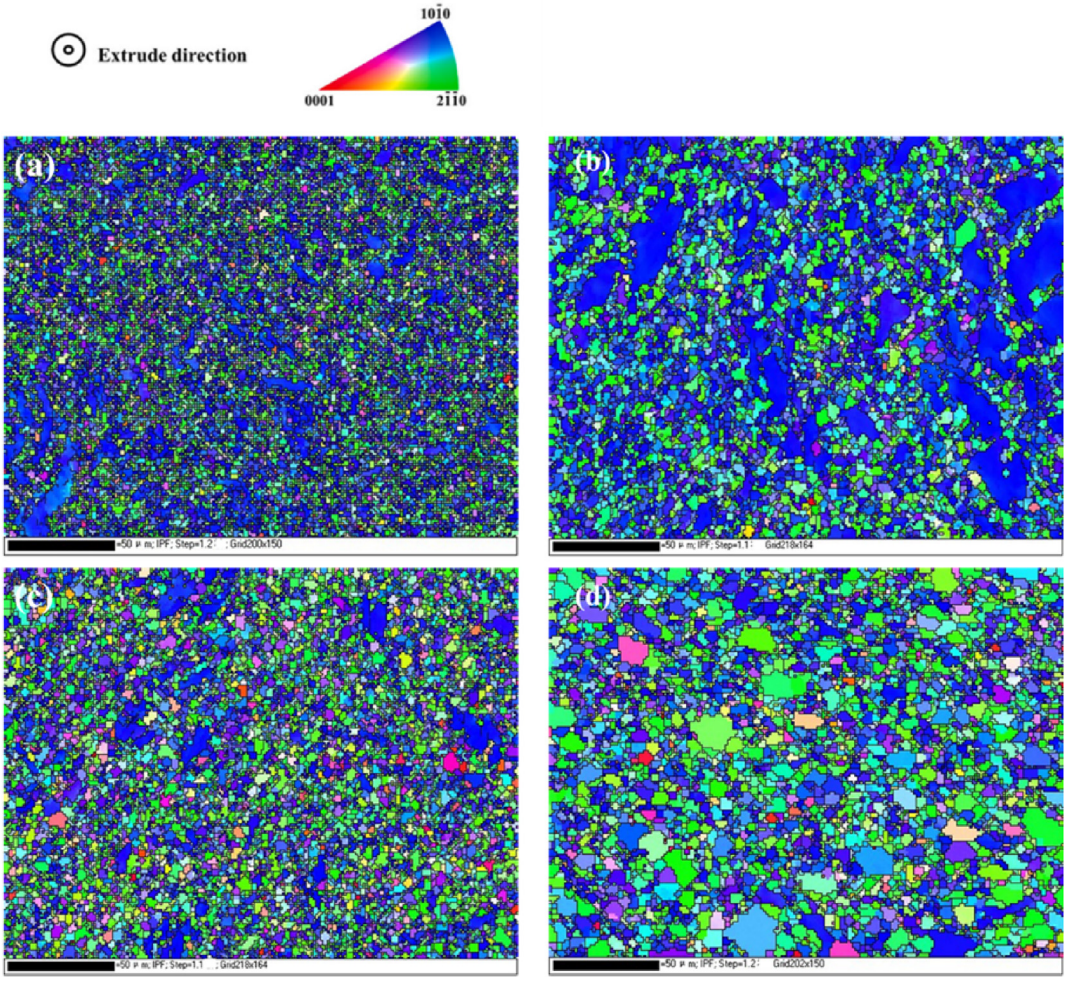

Fig. 12 – The microstructures of four designed alloys obtained by EBSD (IPF results). (a) The AGS of #1 alloy is 0.78 μm; (b) The AGS of #2 alloy is 2.87 μm; (c) The AGS of #3 alloy is 1.97 μm; (d) The AGS of #4 alloy is 4.35 μm.

Table 3 – The results of predictions and experiments.

No.	#1	#2	#3	#4
Predictions of DT	Ultrafine	Ultrafine	Ultrafine	Ultrafine
Predictions of ANN	1.02 μm	3.37 μm	2.19 μm	5.53 μm
Experimental results	0.78 μm Ultrafine	2.87 μm Ultrafine	1.97 μm Ultrafine	4.35 μm Ultrafine

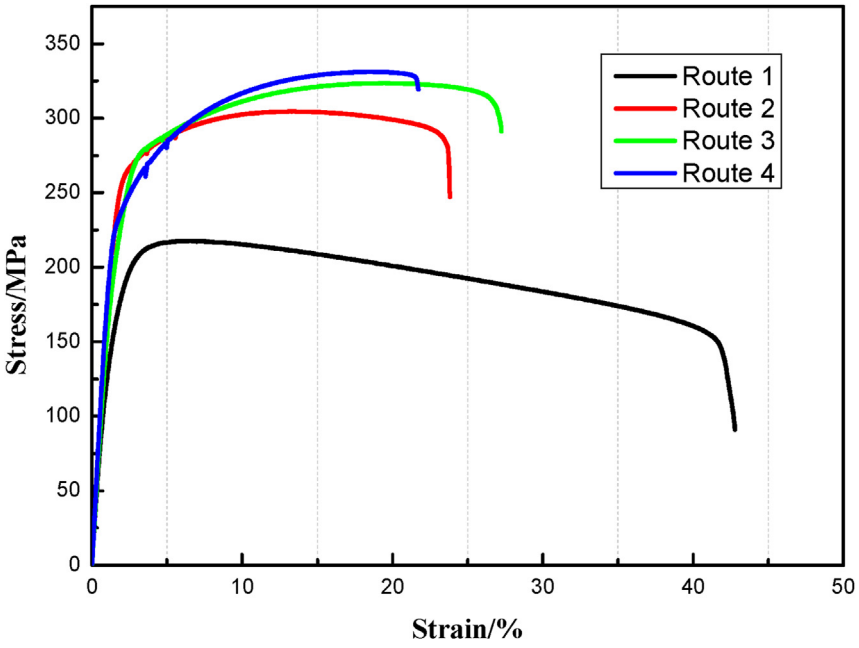

Fig. 13 – Tension engineering stress-strain curves of four alloys.

Fig. 12 shows the microstructures of four designed alloys taken at 500×. Herein, our study adopted the low-angle boundary of 2°–15° and the high-angle boundary of greater than 15° to obtain the IPF results. The white boundaries represent the grain boundaries of uncrystallized grains, while the black boundaries indicate the grain boundaries of recrystallized grains. As shown in Fig. 12, it can be observed that there are very few white boundaries, which implies that the alloys are almost fully recrystallized. After measurement and statistics, the average grain sizes of alloys #1 to #4 were found to be 0.78 μm, 2.87 μm, 1.97 μm, and 4.35 μm, respectively. These are ultrafine grain alloys, indicating that the four routes proposed for designing ultrafine grain are feasible.

Table 3 presents the predictive results from DT and ANN models, along with experimental results representing the actual values. After inputting the composition and extrusion process parameters into the decision tree model, the predicted results were obtained for all ultrafine. Additionally, the ANN model predicted grain sizes of 1.02 μm, 3.37 μm, 2.19 μm, and 5.53 μm when provided with the same parameters. The calculated model accuracy for the ultrafine grain classifier is 100%, which is slightly higher than the model calculation accuracy of 91%. The validation model accuracy of the grain size predictor is 83%, slightly lower than the model calculation accuracy of 89%. The models demonstrate good generalization and predictive performance.

Some mechanical tensile tests were also performed to evaluate the properties of designing alloys. The samples had 25 mm gage lengths and 6 mm × 3 mm cross-sections, and the tensile tests were conducted using a CMT6305-300 KN electronic universal testing machine at a strain rate of $1 \times 10^{-3}\ s^{-1}$ at room temperature. Tensile engineering stress-strain curves of the extruded alloys are shown in Fig. 13. The mechanical properties of these four alloys are very similar to those shown in Fig. 8. Alloy #1 has a higher fracture elongation when prepared using route 1; alloy #4 has a higher ultimate strength prepared using route 4. Alloys #2 and #3 have good comprehensive mechanical properties when prepared using routes 2 and 3, respectively.

5. Conclusions

In this work, we have proposed a new design strategy for ultrafine grain Mg alloys based on machine learning. We found the main factors affecting grain size, designed ultrafine grain preparation routes, and built models to predict grain size using machine learning and data analysis as the primary approaches. Our main findings are summarized as follows.

(1) Four classification models were built by kNN, SVM, RF, and DT algorithms. Their test accuracy is 0.66, 0.78, 0.78,

and 0.79, respectively. Using the DT model, we developed a grain classifier to predict the grain types of new alloys. The training and testing accuracy of the optimized model is 95% and 91%, and the accuracy of the experimental verification is 100%. We also built a predictor of grain size using the ANN algorithm. The training and testing accuracy of the optimized model is 97% and 89%, and the accuracy of the experimental verification exceeds 80%.

(2) For the Mg–Mn-(Al–Zn–Sn–Ca) wrought alloys, we found that the content of Al and extrusion temperature are the two most significant factors influencing the grain size, followed by the content of Mn and Zn. However, the content of Sn, Ca, and extrusion speed have little effect on grain size.

(3) Four routes to prepare ultrafine grain Mg alloys have been obtained by visualizing the decision tree. We also discovered several general rules for preparing ultrafine grains, such as the need to carefully control the extrusion temperature in relation to the content of Zn and Mn, and the need to keep the Al content below 6.95 wt% and the Mn content at most 3.0 wt%.

(4) Four new wrought Mg alloys were developed through the ML models. The experimental results of these alloys were used to validate the accuracy of the ML models and evaluate the feasibility of our design strategy. The results show that the four alloys we designed have ultrafine grains and the expected mechanical properties.

In summary, the ultrafine grain design strategy proposed in this paper has more than 80% accuracy after experimental verification. The conclusions obtained by ML models match with some underlying theories and do more detailed quantitative studies, which gives us new means and good a priori guidance in designing new Mg–Mn-based alloys. It also provides help for large-scale industrial applications of more high-performance and low-cost Mg alloys.

Declaration of competing interest

The authors declare that they have no known competing financial interests or personal relationships that could have appeared to influence the work reported in this paper.

Data availability

The datasets generated and/or analyzed during the current study are available on request.

Acknowledgments

This work was supported by the National Natural Science Foundation of China (51971042, 51901028), the Chongqing Academician Special Fund (cstc2020yszx-jcyjX0001). Xiaoxi Mi (CSC202006050067) is also grateful to the China Scholarship Council (CSC) and Norwegian University of Science and Technology (NTNU) for their financial and technical support.

REFERENCES

[1] Li SB, Yang XY, Hou JT, Du WB. A review on thermal conductivity of magnesium and its alloys. J Magn Alloys 2020;8(1):78–90. https://doi.org/10.1016/j.jma.2019.08.002.

[2] Song JF, She J, Chen DL, Pan FS. Latest research advances on magnesium and magnesium alloys worldwide. J Magn Alloys 2020;8(1):1–41. https://doi.org/10.1016/j.jma.2020.02.003.

[3] Pan HC, Ren YP, Fu H, Zhao H, Wang LQ, Meng XY, et al. Recent developments in rare-earth free wrought magnesium alloys having high strength: a review. J Alloys Compd 2016;663:321–31. https://doi.org/10.1016/j.jallcom.2015.12.057.

[4] Zeng ZR, Stanford N, Davies CHJ, Nie JF, Birbilis N. Magnesium extrusion alloys: a review of developments and prospects. Int Mater Rev 2019;64(1):27–62. https://doi.org/10.1080/09506608.2017.1421439.

[5] Cheng S, Spencer JA, Milligan WW. Strength and tension/compression asymmetry in nanostructured and ultrafine-grain metals. Acta Mater 2003;51(15):4505–18. https://doi.org/10.1016/S1359-6454(03)00286-6.

[6] Greer JR, De Hosson JTM. Plasticity in small-sized metallic systems: intrinsic versus extrinsic size effect. Prog Mater Sci 2011;56(6):654–724. https://doi.org/10.1016/j.pmatsci.2011.01.005.

[7] StJohn DH, Easton MA, Qian M, Taylor JA. Grain refinement of Magnesium alloys: a review of recent research, theoretical developments, and their application. Metall Mater Trans 2013;44:2935–49. https://doi.org/10.1007/s11661-012-1513-x.

[8] Edalati K, Masuda T, Arita M, Furui M, Sauvage X, Horita Z, et al. Room-Temperature superplasticity in an ultrafine-grained Magnesium alloy. Sci Rep 2017;7:2662. https://doi.org/10.1038/s41598-017-02846-2.

[9] Zhilyaev AP, Langdon TG. Using high-pressure torsion for metal processing: fundamentals and applications. Prog Mater Sci 2008;53(6):893–979. https://doi.org/10.1016/j.pmatsci.2008.03.002.

[10] Toth LS, Gu C. Ultrafine-grain metals by severe plastic deformation. Mater Charact 2014;92:1–14. https://doi.org/10.1016/j.matchar.2014.02.003.

[11] Minárik P, Veselý J, Král R, Bohlen J, Kubásek J, Janeček M, et al. Exceptional mechanical properties of ultra-fine grain Mg-4Y-3RE alloy processed by ECAP. Mater Sci Eng, A 2017;708:193–8. https://doi.org/10.1016/j.msea.2017.09.106.

[12] Saito Y, Utsunomiya H, Tsuji N, Sakai T. Novel ultra-high straining process for bulk materials–development of the accumulative roll-bonding (ARB) process. Acta Mater 1999;47(2):579–83. https://doi.org/10.1016/S1359-6454(98)00365-6.

[13] Anne G, Ramesh MR, Nayaka SH, Arya SB, Sahu S. Microstructure evolution and mechanical and corrosion behavior of accumulative roll bonded Mg-2%Zn/Al-7075 multilayered composite. J Mater Eng Perform 2017;26:1726–34. https://doi.org/10.1007/s11665-017-2576-z.

[14] Wang BZ, Liu CM, Gao YH, Jiang SN, Chen ZY, Luo Z. Microstructure evolution and mechanical properties of Mg-Gd-Y-Ag-Zr alloy fabricated by multidirectional forging and ageing treatment. Mater Sci Eng, A 2017;702:22–8. https://doi.org/10.1016/j.msea.2017.06.038.

[15] Wang Y, Rong W, Wu YJ, Peng LM, Chen J, Ding WJ. Effects of Mn addition on the microstructures and mechanical properties of the Mg-15Gd-1Zn alloy. J Alloys Compd 2017;698:1066–76. https://doi.org/10.1016/j.jallcom.2016.12.165.

[16] Yu ZW, Tang AT, Wang Q, Gao ZY, He JJ, She J, et al. High strength and superior ductility of an ultra-fine-grained

magnesium–manganese alloy. Mater Sci Eng, A 2015;648:202–7. https://doi.org/10.1016/j.msea.2015.09.065.
[17] Peng P, He XJC, She J, Tang AT, Rashad M, Zhou SB, et al. Novel low-cost magnesium alloys with high yield strength and plasticity. Mater Sci Eng, A 2019;766:138332. https://doi.org/10.1016/j.msea.2019.138332.
[18] Hu FP, Zhao SJ, Gu GL, Ma ZD, Wei GB, Yang Y, et al. Strong and ductile Mg-0.4Al alloy with minor Mn addition achieved by conventional extrusion. Mater Sci Eng, A 2020;795:139926. https://doi.org/10.1016/j.msea.2020.139926.
[19] Meng SJ, Yu H, Fan SD, Li QZ, Park SH, Suh JS, et al. Recent progress and development in extrusion of rare earth free Mg alloys: a review. Acta Metall Sin 2019;32:145–68. https://doi.org/10.1007/s40195-018-00871-2.
[20] Peng P, Tang AT, Wang B, Zhou SB, She J, Zhang JY, et al. Achieving superior combination of yield strength and ductility in Mg–Mn–Al alloys via ultrafine grain structure. J Mater Res Technol 2021;15:1252–65. https://doi.org/10.1016/j.jmrt.2021.08.133.
[21] Guan HT, Xiao H, Ouyang SH, Tang AT, Chen XH, Tan J, et al. A review of the design, processes, and properties of Mg-based composites. Nanotechnol Rev 2022;11(1):712–30. https://doi.org/10.1515/ntrev-2022-0043.
[22] Peng P, She J, Tang AT, Zhang JY, Zhou SB, Rashad M, et al. A new dilute Mg–Mn–Al alloy with exceptional rollability and ductility at room temperature. Mater Sci Eng, A 2022;859:144229. https://doi.org/10.1016/j.msea.2022.144229.
[23] Yu ZW, Tang AT, He JJ, Gao ZY, She J, Liu JG, et al. Effect of high content of manganese on microstructure, texture and mechanical properties of magnesium alloy. Mater Charact 2018;136:310–7. https://doi.org/10.1016/j.matchar.2017.12.029.
[24] Liao HX, Kim J, Liu TT, Tang AT, She J, Peng P, et al. Effects of Mn addition on the microstructures, mechanical properties and work-hardening of Mg-1Sn alloy. Mater Sci Eng, A 2019;754:778–85. https://doi.org/10.1016/j.msea.2019.02.021.
[25] She J, Pan FS, Guo W, Tang AT, Gao ZY, Luo SQ, et al. Effect of high Mn content on development of ultra-fine grain extruded magnesium alloy. Mater Des 2016;90:7–12. https://doi.org/10.1016/j.matdes.2015.10.093.
[26] Nakata T, Xu C, Ajima R, Matsumoto Y, Shimizu K, Sasaki TT, et al. Improving mechanical properties and yield asymmetry in high-speed extrudable Mg-1.1Al-0.24Ca (wt%) alloy by high Mn addition. Mater Sci Eng, A 2018;712:12–9. https://doi.org/10.1016/j.msea.2017.11.085.
[27] Nakata T, Mezaki T, Ajima R, Xu C, Oh-ishi K, Shimizu K, et al. High-speed extrusion of heat-treatable Mg–Al–Ca–Mn dilute alloy. Scr Mater 2015;101:28–31. https://doi.org/10.1016/j.scriptamat.2015.01.010.
[28] Yu H, Park SH, You BS. Development of extraordinary high-strength Mg–8Al–0.5 Zn alloy via a low temperature and slow speed extrusion. Mater Sci Eng, A 2014;610:445–9. https://doi.org/10.1016/j.msea.2014.05.058.
[29] Choudhary K, DeCost B, Chen C, Jain A, Tavazza F, Cohn R, et al. Recent advances and applications of deep learning methods in materials science. npj Comput Mater 2022;8:59. https://doi.org/10.1038/s41524-022-00734-6.
[30] Ramprasad R, Batra R, Pilania G, Mannodi-Kanakkithodi A, Kim C. Machine learning in materials informatics: recent applications and prospects. npj Comput Mater 2017;3:54. https://doi.org/10.1038/s41524-017-0056-5.
[31] Butler KT, Davies DW, Cartwright H, Isayev O, Walsh A. Machine learning for molecular and materials science. Nature 2018;559:547–55. https://doi.org/10.1038/s41586-018-0337-2.
[32] Holm EA, Cohn R, Gao N, Kitahara AR, Matson TP, Lei B, et al. Overview: computer vision and machine learning for microstructural characterization and analysis. Metall Mater Trans 2020;51:5985–99. https://doi.org/10.1007/s11661-020-06008-4.
[33] Chen T, Gao Q, Yuan Y, Li TY, Xi Q, Liu TT, et al. Coupling physics in machine learning to investigate the solution behavior of binary Mg alloys. J Magn Alloys 2022;10(10):2817–32. https://doi.org/10.1016/j.jma.2021.06.014.
[34] Xue DZ, Balachandran PV, Hogden J, Theiler J, Xue DQ, Lookman T. Accelerated search for materials with targeted properties by adaptive design. Nat Commun 2016;7:11241. https://doi.org/10.1038/ncomms11241.
[35] Zhang HT, Fu HD, He XQ, Wang CS, Jiang L, Chen LQ, et al. Dramatically enhanced combination of ultimate tensile strength and electric conductivity of alloys via machine learning screening. Acta Mater 2020;200:803–10. https://doi.org/10.1016/j.actamat.2020.09.068.
[36] Zhao QK, Yang HY, Liu JB, Zhou HF, Wang HT, Yang W. Machine learning-assisted discovery of strong and conductive Cu alloys: data mining from discarded experiments and physical features. Mater Des 2021;197:109248. https://doi.org/10.1016/j.matdes.2020.109248.
[37] Orme AD, Chelladurai I, Rampton TM, Fullwood DT, Khosravani A, Miles MP, et al. Insights into twinning in Mg AZ31: a combined EBSD and machine learning study. Comput Mater Sci 2016;124:353–63. https://doi.org/10.1016/j.commatsci.2016.08.011.
[38] Tong ZN, Wang LY, Zhu GM, Zeng XQ. Predicting twin nucleation in a polycrystalline Mg alloy using machine learning methods. Metall Mater Trans 2019;50:5543–60. https://doi.org/10.1007/s11661-019-05468-7.
[39] Jung ID, Shin DS, Kim D, Lee J, Lee MS, Son HJ, et al. Artificial intelligence for the prediction of tensile properties by using microstructural parameters in high strength steels. Materialia 2020;11:100699. https://doi.org/10.1016/j.mtla.2020.100699.
[40] Fang LC, Cheng L, Glerum JA, Bennett J, Cao J, Wagner GJ. Data-driven analysis of process, structure, and properties of additively manufactured Inconel 718 thin walls. npj Comput Mater 2022;8:126. https://doi.org/10.1038/s41524-022-00808-5.
[41] Wu X, Jing XR, Xiao H, Ouyang SH, Tang AT, Peng P, et al. Controlling grain size and texture in Mg–Zn–Mn alloys from the interaction of recrystallization and precipitation. J Mater Res Technol 2022;21:1395–407. https://doi.org/10.1016/j.jmrt.2022.09.108.
[42] Mi XX, Tian LJ, Tang AT, Kang J, Peng P, She J, et al. A reverse design model for high-performance and low-cost magnesium alloys by machine learning. Comput Mater Sci 2022;201:110881. https://doi.org/10.1016/j.commatsci.2021.110881.
[43] She J, Pan FS, Peng P, Tang AT, Yu ZW, Wu L, et al. The microstructure and mechanical properties of Mg-xAl -5Sn-0.3Mn (x=1, 3, 6 and 9) series alloys. Mater Sci Technol 2015;31:344–8. https://doi.org/10.1179/1743284714Y.0000000540.
[44] Jiang MG, Xu C, Nakata T, Yan H, Chen RS, Kamado S. Development of dilute Mg–Zn–Ca–Mn alloy with high performance via extrusion. J Alloys Compd 2016;668:13–21. https://doi.org/10.1016/j.jallcom.2016.01.195.
[45] Zhang AY, Kang R, Wu L, Pan HC, Xie HB, Huang QY, et al. A new rare-earth-free Mg-Sn-Ca-Mn wrought alloy with ultra-high strength and good ductility. Mater Sci Eng, A 2019;754:269–74. https://doi.org/10.1016/j.msea.2019.03.095.
[46] Pan FS, Mao JJ, Zhang G, Tang AT, She J. Development of high-strength, low-cost wrought Mg–2.0mass% Zn alloy with high Mn content. Prog Nat Sci: Mater Int 2016;26(6):630–5. https://doi.org/10.1016/j.pnsc.2016.11.016.

[47] Zhang DF, Shi GL, Dai QW, Yuan W, Duan H. Microstructures and mechanical properties of high strength Mg-Zn-Mn alloy. Trans Nonferrous Metals Soc China 2008;18:s59–63. https://doi.org/10.1016/S1003-6326(10)60175-6.
[48] Luo AA, Sachdev AK. Development of a new wrought magnesium-aluminum- manganese alloy AM30. Metall Mater Trans 2007;38(6):1184–92. https://doi.org/10.1007/s11661-007-9129-2.
[49] Peng P, She J, Tang AT, Zhang JY, Song K, Yang QS, et al. A strategy to regulate the microstructure and properties of Mg-2.0 Zn-1.5 Mn magnesium alloy by tracing the existence of Mn element. J Alloys Compd 2022;890:161789. https://doi.org/10.1016/j.jallcom.2021.161789.
[50] Valiev RZ, Langdon TG. Principles of equal-channel angular pressing as a processing tool for grain refinement. Prog Mater Sci 2006;51(7):881–981. https://doi.org/10.1016/j.pmatsci.2006.02.003.
[51] Cheng S, Spencer JA, Milligan WW. Strength and tension/compression asymmetry in nanostructured and ultrafine-grain metals. Acta Mater 2003;51(15):4505–18. https://doi.org/10.1016/S1359-6454(03)00286-6.
[52] Song R, Ponge D, Raabe D, Speer JG, Matlock DK. Overview of processing, microstructure and mechanical properties of ultrafine grained bcc steels. Mater Sci Eng, A 2006;441(1–2):1–17. https://doi.org/10.1016/j.msea.2006.08.095.
[53] Miller RL. Ultrafine-grained microstructures and mechanical properties of alloy steels. Metall Mater Trans B 1972;3:905–12. https://doi.org/10.1007/BF02647665.
[54] Figueiredo RB, Sabbaghianrad S, Giwa A, Greer JR, Langdon TG. Evidence for exceptional low temperature ductility in polycrystalline magnesium processed by severe plastic deformation. Acta Mater 2017;122:322–31. https://doi.org/10.1016/j.actamat.2016.09.054.
[55] Fan HD, Aubry S, Arsenlis A, El-Awady JA. Grain size effects on dislocation and twinning mediated plasticity in magnesium. Scr Mater 2016;112:50–3. https://doi.org/10.1016/j.scriptamat.2015.09.008.
[56] Liu BY, Liu F, Yang N, Zhang L, Yang Y, Li B, et al. Large plasticity in magnesium mediated by pyramidal dislocations. Science 2019;365(6448):73–5. https://www.science.org/doi/10.1126/science.aaw2843.
[57] Singh A, Osawa Y, Somekawa H, Mukai T. Ultra-fine grain size and isotropic very high strength by direct extrusion of chill-cast Mg–Zn–Y alloys containing quasicrystal phase. Scr Mater 2011;64(7):661–4. https://doi.org/10.1016/j.scriptamat.2010.12.016.
[58] Song D, Ma AB, Jiang JH, Lin PH, Yang DH, Fan JH. Corrosion behavior of equal-channel-angular-pressed pure magnesium in NaCl aqueous solution. Corros Sci 2010;52(2):481–90. https://doi.org/10.1016/j.corsci.2009.10.004.
[59] Pedregosa F, Varoquaux G, Gramfort A. Scikit-learn: machine learning in Python. J Mach Learn Res 2011;12:2825–30. http://scikit-learn.sourceforge.net.
[60] Chen T, Yuan Y, Mi XX, Wu JJ, Tang AT, Wang JF, et al. Interaction of elements in dilute Mg alloys: a DFT and machine learning study. J Mater Res Technol 2022. https://doi.org/10.1016/j.jmrt.2022.11.071.
[61] Schmidhuber J. Deep learning in neural networks: an overview. Neural Network 2015;61:85–117. https://doi.org/10.1016/j.neunet.2014.09.003.
[62] LeCun Y, Bengio Y, Hinton G. Deep learning. Nature 2015;521(7553):436–44. https://doi.org/10.1038/nature14539.